The effect of small elongations on the electronic and optical signatures in InAs nanocrystal quantum dots

2009 J. Phys.: Condens. Matter 21 144212

(http://iopscience.iop.org/0953-8984/21/14/144212)

IOP Publishing Journal of Physics: Condensed Matter

J. Phys.: Condens. Matter **21** (2009) 144212 (5pp) doi:10.1088/0953-8984/21/14/144212

The effect of small elongations on the electronic and optical signatures in InAs nanocrystal quantum dots

T Puangmali, Marco Califano and P Harrison

Institute of Microwaves and Photonics, School of Electronic and Electrical Engineering, University of Leeds, Leeds LS2 9JT, UK

E-mail: m.califano@leeds.ac.uk

Received 8 July 2008, in final form 29 September 2008
Published 18 March 2009
Online at stacks.iop.org/JPhysCM/21/144212

Abstract

We present a detailed theoretical investigation of the electronic structure and optical properties of InAs nanocrystals at the transition from spheres to rods. Using a semiempirical pseudopotential approach, we predict that, despite the qualitative similarity of both intra- and inter-band optical spectra, for NCs with $R > 15$ Å even slight elongations should result in shifts of the order of hundreds of meV in the spacings between STM peaks measured in the positive bias regime, in the position of the intra-band absorption peaks associated with transitions within the conduction band and in the separation between the first and the fifth peak in PLE experiments. Our results show that, based on the spectroscopic data, it should be possible to discriminate between spherical and elongated NCs with aspect ratios of length over diameter as small as 1.2. Indeed our results suggest that many nominally spherical experimental samples contained a large fraction of slightly elongated structures.

(Some figures in this article are in colour only in the electronic version)

1. Introduction

The identification of the rich absorption features observed in optical spectroscopy on nanocrystal (NC) ensembles, in terms of specific excitonic state components, is a complex issue. Many different factors contribute to the uncertainty of their assignment; size and shape distributions being the most significative. In fact, although experimentalists nowadays always have access to microscopic information (usually in the form of transmission electron microscopy (TEM) or its high-resolution version), often complemented by x-ray scattering, these methods are not completely reliable and may underestimate the actual dimensions, being insensitive to non-periodic layers at the NC surface [1]. Furthermore the TEM images only show *cross sections* on a specific plane, from which little information can be extracted on the perpendicular direction. Therefore there is always some degree of ambiguity on both the size and shape of the NCs even when micrographs are supplied.

Here we investigate the effects of small elongations on the spectroscopic features in InAs NCs. These particles have attracted great interest as their optical properties can be tuned with size to cover the technologically important energy window between the visible and the near infrared [2], making them potentially ideally suited for applications in biology [3], electro-optics [4] and telecommunications [5]. Furthermore due to the large difference between the electron and hole effective masses in InAs, they are expected to exhibit highly efficient carrier multiplication. This process, where multiple excitons are generated upon absorption of a single photon [6], has important implications for the application of NCs in photovoltaics [7], as it can greatly increase the photocurrent output of the device. From this point of view, the knowledge of the NC shape is very important, as it may affect the efficiency of both carrier multiplication and carrier collection (i.e. how efficiently electrons and holes travel to the electrodes after they have been separated to generate a photocurrent).

We show that the intra- and inter-band optical absorption spectra calculated for spherical NCs, although qualitatively similar to those relative to slightly elongated structures either with the same radius, or containing the same total number of constituent atoms, exhibit specific quantitative signatures

which allow one to distinguish between the two shapes. Elongated structures are found to exhibit large red shifts in the position of the peak associated with the intra-band transition between the two lowermost levels in the conduction band and in the energy separation between the first and the fifth peak in inter-band absorption spectra. Shifts of the same order of magnitude (hundreds of meV) are also predicted in the spacings between STM peaks measured in the positive bias regime. This information can be valuable in determining the substantial presence of even slightly elongated structures in experimental samples of 'nominally' spherical NCs.

2. Method

We consider As-centred InAs spherical (quantum dots, QDs) and elongated (quantum rods, QRs) NCs with the zincblende structure (lattice constant $a = 6.0584$ Å), constructed by adding successive atomic layers up to a specific cutoff radius $r_{\rm cut}$ (and cutoff length $l_{\rm cut}$ along the z (001) direction for elongated structures). This procedure leaves some of the atoms on the NC surface with unsatisfied (dangling) bonds. Surface atoms with only one bond (i.e., three dangling bonds) are systematically removed. The effective radius of a dot (R) is defined in terms of the total number of In and As atoms in the dot ($N_{\rm dot}$) as $R = a(\Omega N_{\rm dot})^{1/3}$, where $\Omega = 3/(32\pi)$ for the zincblende crystal structure. The effective radius of a rod is assumed to be equal to that of the dot with the same value of $r_{\rm cut}$. The dangling bonds at the NC surface (maximum two per atom) are passivated by pseudo-hydrogen atoms, located at a distance ηd_0 ($0 < \eta < 1$) from the centre of the passivated atom along the direction of the ideal bulk In–As bond of length d_0. The ligand potentials have a Gaussian form

$$v(\boldsymbol{r}) = \alpha {\rm e}^{-(|\boldsymbol{r}-\boldsymbol{R}_{\rm p}|/\beta)^2}, \tag{1}$$

where $\boldsymbol{R}_{\rm p} = \boldsymbol{R}_{\rm p}(\eta)$ is the location of the passivants, α and β represent, respectively, the amplitude and width of the Gaussian potential. As our electronic structure calculations are performed in reciprocal space, we use the Fourier transform of (1):

$$v(\boldsymbol{q}) = a{\rm e}^{{\rm i}\boldsymbol{q}\cdot\boldsymbol{R}_{\rm p}}{\rm e}^{-(b|\boldsymbol{q}|)^2} \tag{2}$$

where $a \equiv \alpha\pi^{1.5}\beta^3$ and $b \equiv \beta/2$. This 12-parameter set (represented by a, b and η for anions and cations with one and two dangling bonds) is optimized on flat (001- 110- 111-oriented slabs) and curved (dots) test structures, using an automated method [8], based on the global optimization algorithm DIRECT [9]. The quality of a passivation is determined by the extent to which the lowermost n states in the conduction band and uppermost m states in the valence band are *not* on the NC surface. A measure of this could be the position of the energy levels with respect to the band gap. However a more stringent test yielding a more quantitative estimate is obtained by integrating the wavefunctions squared across the interior of each test structure.

We selected the four sets yielding the best passivation according to this criterion and calculated the single-particle gap and the energy separation between the two uppermost (lowermost) states in the valence (conduction) band. The difference in the results was found to be negligible, showing the independence of the calculated values on the choice of the passivation parameters. We therefore selected the set with highest quality factor (see table 1).

Table 1. Passivation parameters used in the calculations (the values are in atomic units). ci and ai refer, respectively, to cations and anions with $i = 1, 2$ dangling bonds.

	c1	c2	a1	a2
a	1.965	1.965	−1.144	−1.050
b	0.177	0.592	0.575	0.783
η	0.572	0.705	0.250	0.250

The single-particle states of a NC were obtained using the *folded spectrum method* [10] in which the conventional Schrödinger equation is replaced by

$$\left[-\tfrac{1}{2}\nabla^2 + V(r) + V_{\rm nl} - \varepsilon_{\rm ref}\right]^2 \psi_i(r) = (\varepsilon_i - \varepsilon_{\rm ref})^2\,\psi_i(r) \tag{3}$$

where $V_{\rm nl}$ accounts for the non-local part of the potential (including spin–orbit) and the local potential $V(r)$ is obtained as a superposition of screened atomic pseudopotentials [11] for each atom species α:

$$V(r) = \sum_{n,\alpha} V_\alpha(|r - R_{n,\alpha}|). \tag{4}$$

Equation (3) is solved, using periodic boundary conditions, by expanding the pseudopotential wavefunctions in a plane-wave basis set. This provides selected eigensolutions of the Schrödinger equation with energy close to an arbitrarily chosen reference energy $\varepsilon_{\rm ref}$.

The excitonic wavefunctions $\Psi^{(\gamma)}$ (where γ denotes the exciton quantum numbers) are expanded as a linear combination of single substitution Slater determinants $\Phi_{v,c}$ constructed with the single-particle wavefunctions $\psi_i(r)$ solutions of (3). The matrix elements of the many-body Hamiltonian in this basis set include the electron–hole direct and exchange Coulomb integrals [12], which are calculated using the single-particle wavefunctions solution of (3) and a size- and position-dependent microscopic dielectric function $\epsilon(r_1, r_2)$ [12].

The optical absorption spectrum is then calculated as

$$I(E) = \frac{1}{V}\sum_{\gamma} |M^{(\gamma)}|^2 {\rm e}^{-\left(\frac{E-E^{(\gamma)}}{\Gamma}\right)^2}. \tag{5}$$

$E^{(\gamma)}$ are the exciton energies, Γ represents an experimental line broadening and $M^{(\gamma)}$ are the dipole matrix elements:

$$M^{(\gamma)} = \sum_{v,c} A_{v,c}^{(\gamma)} \langle \psi_v | \boldsymbol{r} | \psi_c \rangle \tag{6}$$

where the coefficients $A_{v,c}^{(\gamma)}$ are the eigenstates of the many-body Hamiltonian.

This approach (and very similar EPM-based ones) has proved highly successful in the past in interpreting the optical properties of spherical nanostructures made of different materials such as CdSe [12, 13], InP [12, 14], PbSe [15], and InAs [16, 17]. However, so far it had been applied to the investigation of *elongated* NCs made of CdSe [18] and InP only [19].

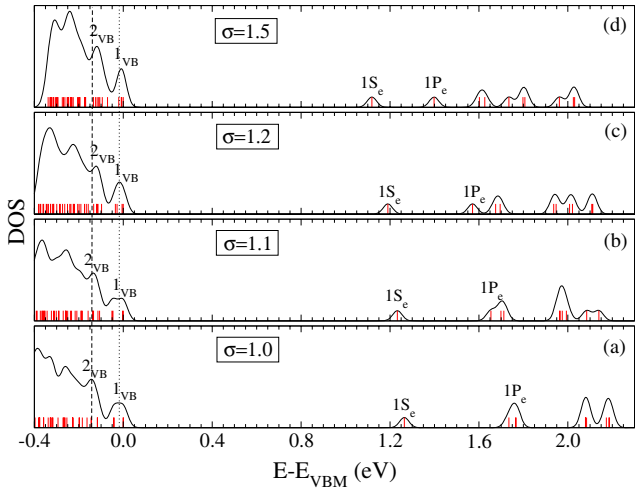

Figure 1. Density of states calculated for four InAs NCs with $R = 20$ Å and $\sigma = 1$ (a), 1.1 (b), 1.2 (c) and 1.5 (d) using a broadening of 30 meV. The 40 (10) uppermost (lowermost) states in the valence (conduction) band are included (red vertical lines). The dotted and dashed lines mark the position of the first two DOS peaks in a spherical dot (a), allowing comparison with the position of those peaks in the two elongated structures. The labels mark the DOS peaks which could correspond to the state assignment made in [20] (see the text).

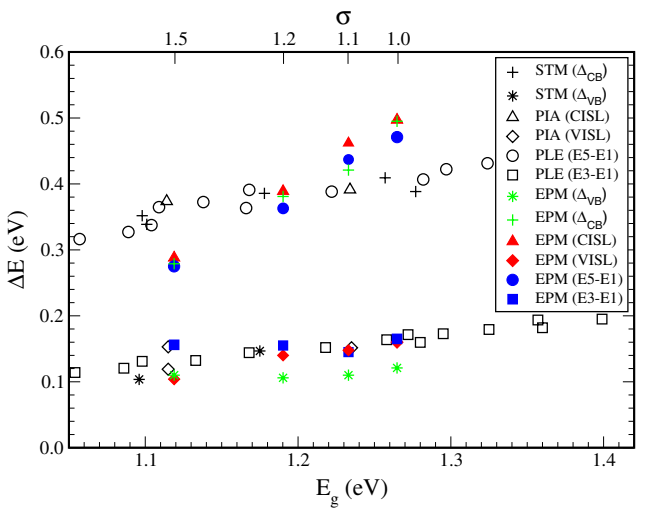

Figure 2. Comparison of the spacings between dos peaks (green crosses and stars), intra-band transition energies (red solid diamonds and triangles) and inter-band E5–E1 and E3–E1 energy spacings (blue solid circles and squares) calculated with the EPM approach and the experimental STM peak separations (black crosses and stars, digitally extracted from figure 3(b) in [20]), the valence and conduction inter-sublevel transition energies measured by PIA (empty diamonds and triangles, digitally extracted from figure 2 in [22]) and the E5–E1 and E3–E1 separations between the measured PLE peaks (empty circles and squares, digitally extracted from figure 3(b) in [20]), see the text, as a function of the single-particle energy gap.

3. Results and discussion

Using the Hamiltonian described above, we calculated the electronic structure of InAs QDs with effective radii $R_{QD} =$ 14.6 (465), 20 (1207), 21.7 (1547) and 24.1 (2115) and 25.8 (2590) Å (where the quantities in brackets denote the number of constituent atoms N_a for each NC) and QRs with radii $R_{QR} = 14.6$ and 20 Å and aspect ratios $\sigma = L/2R_{QR}$ ranging from 1 to 1.5 (with corresponding values of $1207 < N_a < 2200$ for the 20 Å rod). In figure 1 we show the density of states (DOS) for the uppermost 40 states in the valence band and the lowermost 10 states in the conduction band calculated for four NCs with $R = 20$ Å and $\sigma = 1$, 1.1, 1.2 and 1.5 (the energies are relative to the valence band maximum, VBM). We see that the elongation has two main effects: as σ increases, the density of states in both conduction and valence bands increases and the single-particle band gap E_g shifts to the red.

We have questioned in the past [17] the simple interpretation of the STM peaks measured by Banin *et al* [20] for negative bias, in terms of tunnelling between single-hole states. We found, as in the case of previous tight binding calculations [21], that the spacing between the two uppermost valence band states (ranging from 20 to 40 meV for the NC sizes considered here) was too small compared to the experimental data. Based on the assumption of state-independent quasi-particle polarization self-energies, we proposed an alternative interpretation of the STM results in terms of the spacing between the DOS peaks we calculated for InAs dots [17]. In this approximation, therefore, the calculated DOS for elongated structures shown in figure 1 could provide some insight into the nature of the experimental samples. From figure 1 we see that the spacing Δ_{CB} between the peaks labelled $1S_e$ and $1P_e$ decreases significantly with increasing σ, implying smaller values for the STM peak separations measured on elongated samples. The shift in the position of the VB peaks 1_{VB} and 2_{VB} is less dramatic (with magnitudes of the order of 10% or less of the calculated peak spacing for a spherical NC), and is non-monotonic, their separation Δ_{VB} decreasing for $1 < \sigma \leqslant 1.2$ and then increasing again for more elongated structures. The expected energy shifts are 74, 114 and 216 meV (11, 15 and 11 meV) for the spacings obtained in the positive (negative) bias range with NC with $\sigma = 1.1$, 1.2 and 1.5, respectively, when compared with those relative to spherical structures ($\sigma = 1$) for NCs with $R = 20$ Å. We find a similar qualitative behaviour in the case of smaller NCs ($R = 14.6$ Å). However in this case Δ_{CB} is almost constant up to $\sigma = 1.2$ and decreases by 120 meV for $\sigma = 1.5$, whereas the decrease of Δ_{VB} is larger (50 meV) for $\sigma = 1.2$. Our calculated values for Δ_{VB} and Δ_{CB} are compared with the STM data in figure 2. Although the agreement with the experimental data obtained in the negative bias regime (low energy curve) is good for all values of $1 \leqslant \sigma \leqslant 1.5$, the comparison with the peak spacings in the CB seems to suggest a slight elongation (with $\sigma \leqslant 1.2$) in the experimental samples.

The increase in the single-particle DOS with elongation is also expected to affect the position of the peaks associated with inter-sublevel (ISL) transitions in the NCs. The two well separated features found by Krapf *et al* [22] in their photoinduced absorption (PIA) spectra of InAs colloidal QDs have in fact been associated with ISL transitions between the two lowermost states in the conduction band (CISL, the high

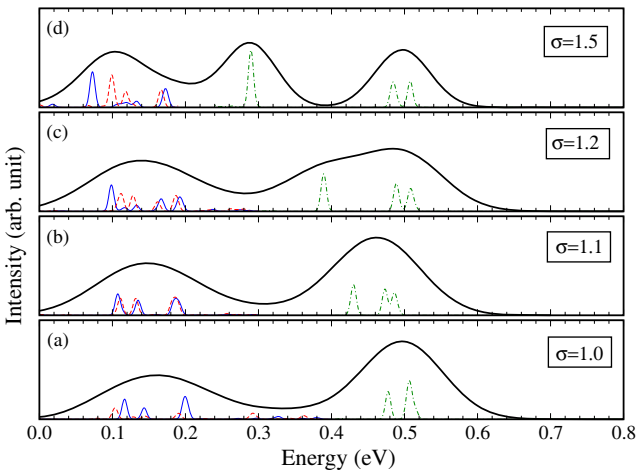

Figure 3. Optical intra-band absorption spectra calculated for InAs NCs with $R = 20$ Å and $\sigma = 1.0$ (a), 1.1 (b), 1.2 (c) and 1.5 (d) using a broadening of 75 meV (thick black line) and 10 meV (coloured thin lines). The thin blue (red dashed) line represents the contribution from VISL transitions originating from the VBM (VBM-1) state.

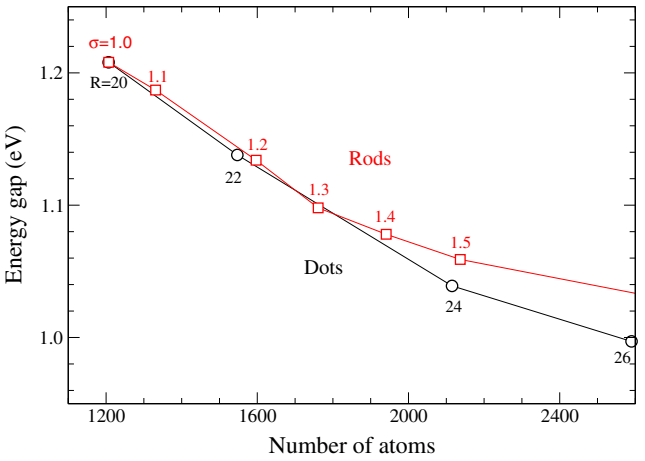

Figure 4. Comparison between the room temperature optical energy gaps calculated for spherical (black circles) and elongated structures (red squares) as a function of the number of atoms in the NC. The value of the dot radius R and the rod aspect ratio σ are also reported. The smallest structure is an InAs NCs with $R = 20$ Å and $\sigma = 1$.

energy peak), and between the two uppermost valence states (VISL, the low energy peak). We therefore predict a similar red shift for these two PIA peaks in elongated NCs, as expected for the STM peak spacings discussed above. Our calculated intra-band absorption spectra relative to NCs with $R = 20$ Å and $1 \leqslant \sigma \leqslant 1.5$ are shown in figure 3. As σ increases both peaks exhibit progressive red shifts, as expected. It is particularly interesting to note the shape evolution of the high energy peak where, for $\sigma = 1.2$, a broad shoulder appears on the low energy side. This feature further develops into a separate peak for larger elongations. Careful examination of the data reported in [22] also reveals the presence of this shoulder in the experimental spectra obtained for NCs with $R \leqslant 24$ Å. As no shoulder is found in our spectra for spherical NCs of any size, its presence could be interpreted as an indication of the substantial presence of slightly elongated structures (with $\sigma \leqslant 1.2$) in the experimental samples (whereas a simple size distribution in spherical NCs would only result in a broadening of the peak), in agreement with our earlier conclusion based on the comparison with STM data. That this might indeed be the case is also suggested by the results of the comparison between the calculated and the observed [22] position of the two intra-band absorption features, shown in figure 2. The values calculated for slightly elongated structures with $1 < \sigma \leqslant 1.2$ show a better agreement with experiment than those obtained for spherical NCs ($\sigma = 1$), in the case of CISL transitions. The presence of elongated NCs would therefore explain the poorer agreement with experiment found in the pseudopotential calculations for spherical NCs of [17] for all quantities related to transitions involving the first excited electron state $1P_e$ (such as the position of the CISL transition peak and the energy separation between the first and fifth peak in the inter-band absorption spectra), if compared to the very good agreement achieved for intra- and inter-band transitions involving all VB states up to the 1 S state in the CB, whereas it would not provide more insight into the observed [22] temperature dependence of the VISL peak, as the contributions from both VBM (thin blue line in figure 3) and VBM-1 (red dashed line) would still be present at low temperature for all values of σ considered.

To further investigate this hypothesis we calculated the evolution of the energy gap from a spherical dot with $R = 20$ Å and $\sigma = 1$ (total number of In and As atoms $N_a = 1207$), to NC structures with $N_a \sim 2200$, obtained by increasing either R up to 24 Å, and keeping σ fixed (dots) or by increasing σ up to 1.5 and keeping R constant (rods). The results are shown in figure 4. We choose to plot E_g as a function of the total number of atoms in the NC since this quantity can often be controlled in the experiment, based on the chemistry of the synthetic process, although, as discussed above, the information on how the atoms are distributed in the NC may be more difficult to obtain. We find that rods exhibit a stronger confinement-induced effect compared with dots with the same value of N_a, as expected. This shows that the confinement in the direction perpendicular to the long axis (i.e., the smaller dimension) provides the dominant contribution to the energy shift, as is the case in epitaxially-grown InAs islands. The value of E_g for QRs with such small aspect ratios is, however, very close to that calculated for spherical NCs with the same number of atoms, their difference remaining $\leqslant$20 meV for $\sigma \leqslant 1.5$. For small values of σ, therefore, the knowledge of E_g alone would be insufficient to determine the NC shape, even in the presence of microscopic information. With the resolution available with TEM, in fact, dots would probably be indistinguishable from rods with small aspect ratios, (especially if the latter were viewed perpendicularly to the long axis), and the radii of dots with similar E_g (R_{QD} between 20 and about 23 Å) would be within ~15% or less of those of the rods ($R_{QR} = 20$ Å), the standard size distribution in experiments being of about 13%.

We therefore calculated the full absorption spectrum, looking for shape-specific signatures. Figure 5 shows the evolution of the optical features as the NC becomes either progressively elongated (as σ increases), keeping R

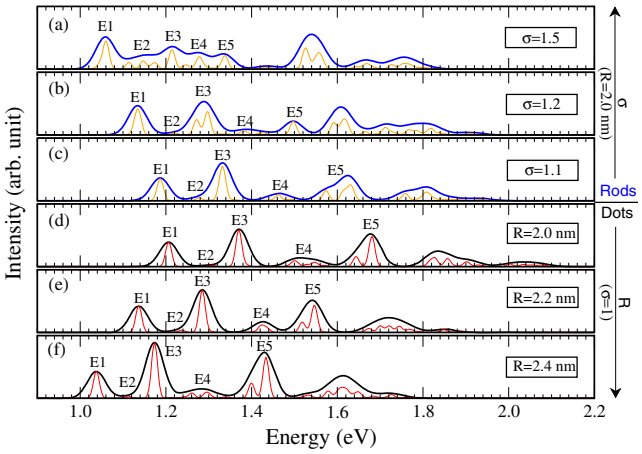

Figure 5. Optical absorption spectra calculated for InAs NCs with $R = 20$ Å and $\sigma = 1.5$ (a), 1.2 (b), 1.1 (c) and 1.0 (d) and dots ($\sigma = 1$) with $R = 21.7$ (e) and 24.1 Å (f), using a broadening of 30 meV (black and blue thick lines) and 10 meV (red and orange thin lines).

constant (=20 Å), or progressively larger (as R increases), keeping σ constant (=1). We see that in all the spectra for $\sigma < 1.5$ three strong peaks can be distinguished, separated by weaker peaks, in qualitative agreement with the experimental findings of [23], whereas the spectrum calculated for a rod with $\sigma = 1.5$ presents substantial differences from that of less elongated structures. In figure 2 we compare the energy separation between the peaks labelled E5 and E1 and those labelled E3 and E1 in the absorption spectra of figure 5 with the corresponding quantities obtained from the experimental size selected PLE spectra measured by Banin *et al* [23]. Once more, in the case of transitions involving the first excited state in the conduction band, a better agreement with experiment is achieved with data calculated for elongated NCs. Based on all the results presented here we can therefore conclude that the experimental samples contained a majority of slightly elongated particles, with $\sigma \leqslant 1.2$.

4. Conclusions

Using a semiempirical pseudopotential approach, we have calculated the effect of small elongations on the electronic and optical features of InAs colloidal dots. We found that although NCs with aspect ratios of length over diameter $\leqslant 1.2$ show qualitatively similar optical spectra, spherical structures can be distinguished from elongated ones based on spectral features related to the energy separation between the 1S and 1P levels in the CB, such as the shape and position of the high energy peak in PIA experiments, the spacing between the first and the fifth peak observed in PLE measurements or the spacing between STM peaks measured in the positive bias regime. Based on the comparison of our results with STM, PIA and PLE data we concluded that the nominally spherical samples used in many experiments contained a significant fraction of slightly elongated particles. The substantial presence of the latter explains the poor agreement with experiment found in previous pseudopotential calculations, for the position of the peaks relative to CISL transitions in PIA spectra and for the magnitude of the E5–E1 separation in PLE spectra.

Acknowledgments

We are grateful to Alex Zunger for granting us permission to use the NanoPSE computational package developed at the National Renewable Energy Lab. (Golden, CO, US) for all the calculations performed here. We would like to thank Peter Graf for kindly providing the code used for the NC passivation and for his precious help and advice in the passivation procedure. TP thanks the Thai government for financial support. MC gratefully acknowledges the Royal Society for financial support under the URF scheme.

References

[1] Murray C B 1995 *PhD Thesis* Chemistry Department, MIT, Cambridge, MA, p 933
[2] Aharoni A, Mokari T, Popov I and Banin U 2006 *J. Am. Chem. Soc.* **128** 257
[3] Michalet X, Pinaud F F, Bentolila L A, Tsay J M, Doose S, Li J J, Sundaresan G, Wu A M, Gambhir S S and Weiss S 2005 *Science* **307** 538
[4] Olsson Y K, Chen G, Rapaport R, Fuchs D T, Sundar V C, Steckel J S, Bawendi M G, Aharoni A and Banin U 2004 *Appl. Phys. Lett.* **85** 4469
[5] Tessler N, Medvedev V, Kazes M, Kan S-H and Banin U 2002 *Science* **295** 1506
[6] Schaller R D and Klimov V I 2004 *Phys. Rev. Lett.* **92** 186601
[7] Nozik A J 2002 *Physica* E **14** 115
[8] Graf P A, Kim K, Jones W B and Wang L W 2007 *J. Comput. Phys.* **224** 824
[9] Jones D R, Perttunen C D and Stuckman B E 1993 *J. Optim. Theory Appl.* **79** 157
[10] Wang L-W and Zunger A 1994 *J. Chem. Phys.* **100** 2394
[11] Magri R and Zunger A 2002 *Phys. Rev.* B **65** 165302
[12] Franceschetti A, Fu H, Wang L-W and Zunger A 1999 *Phys. Rev.* B **60** 1819
[13] Wang L-W and Zunger A 1996 *Phys. Rev.* B **53** 9579
Wang L-W and Zunger A 1998 *J. Phys. Chem.* B **102** 6449
Califano M, Franceschetti A and Zunger A 2005 *Nano Lett.* **5** 2360
Califano M, Franceschetti A and Zunger A 2007 *Phys. Rev.* B **75** 115401
[14] Fu H and Zunger A 1998 *Phys. Rev.* B **57** R15064
Fu H and Zunger A 1997 *Phys. Rev.* B **56** 1496
[15] An J M, Franceschetti A and Zunger A 2007 *Nano Lett.* **7** 2129
An J M, Franceschetti A and Zunger A 2007 *Phys. Rev.* B **76** 161310
[16] Williamson A J and Zunger A 2000 *Phys. Rev.* B **61** 1978
[17] Puangmali T, Califano M and Harrison P 2008 *Phys. Rev.* B at press
[18] Hu J, Li L-S, Yang W, Manna L, Wang L-W and Alivisatos A P 2001 *Science* **292** 2060
Li J and Wang L-W 2003 *Nano Lett.* **3** 101
Califano M, Bester G and Zunger A 2003 *Nano Lett.* **3** 1197
Zhao Q, Graf P A, Jones W B, Franceschetti A, Li J B, Wang L-W and Kim K 2007 *Nano Lett.* **7** 3274
[19] Li J B and Wang L-W 2004 *Nano Lett.* **4** 29
[20] Banin U, Cao Y W, Katz D and Millo O 1999 *Nature* **40** 452
[21] Niquet Y M, Delerue C, Lannoo M and Allan G 2001 *Phys. Rev.* B **64** 113305
[22] Krapf D, Kan S-H, Banin U, Millo O and Saar A 2004 *Phys. Rev.* B **69** 073301
[23] Banin U, Lee C J, Guzelian A A, Kadavanich A V, Alivisatos A, Jaskolski W, Efros A L and Rosen M 1998 *J. Chem. Phys.* **109** 2306